

PAPER

The magnetic structure of DyFeO_3 revisited: Fe spin reorientation and Dy incommensurate magnetic order

To cite this article: Clemens Ritter *et al* 2022 *J. Phys.: Condens. Matter* **34** 265801

View the [article online](#) for updates and enhancements.

You may also like

- [Spin reorientation transition and coupled spin-lattice dynamics of \$\text{Sm}_{0.6}\text{Dy}_{0.4}\text{FeO}_3\$](#)
Azam Ali Khan, Anju Ahlawat, A Sharma et al.
- [Electrochemical Preparation of \$\text{DyFe}_2\$ Alloy from the Solid Mixture of \$\text{Dy}_2\text{O}_3\$ and \$\text{Fe}_2\text{O}_3\$ in Molten \$\text{CaCl}_2\$](#)
Chenming Fan, Guoqing Li, Xiaolong Liu et al.
- [Engineering irreversibility of exchange springs in antiferromagnetic \$\text{DyFe}_2/\text{YFe}_2\$ superlattices](#)
D Wang, A R Buckingham, G J Bowden et al.



IOP | ebooks™

Bringing together innovative digital publishing with leading authors from the global scientific community.

Start exploring the collection—download the first chapter of every title for free.

The magnetic structure of DyFeO₃ revisited: Fe spin reorientation and Dy incommensurate magnetic order

Clemens Ritter^{1,*}, Rui Vilarinho², Joaquim Agostinho Moreira²,
Matus Mihalik³, Marian Mihalik³ and Stanislav Savvin¹

¹ Institut Laue-Langevin, 71 Avenue des Martyrs, 38042 Grenoble, France

² IFIMUP—Institute of Physics for Advanced Materials, Nanotechnology and Photonics, Physics and Astronomy Department, Faculty of Science, University of Porto, Porto, Portugal

³ Institute of Experimental Physics, Watsonova 47, 040 01 Kosice, Slovakia

E-mail: ritter@ill.fr

Received 8 February 2022, revised 6 April 2022

Accepted for publication 14 April 2022

Published 28 April 2022



Abstract

High resolution and high intensity neutron powder diffraction is used to study the ground state magnetic order and the spin reorientation transition in the orthoferrite DyFeO₃. The transition from the high temperature $k = 0 \Gamma_4$ ($G_x A_y F_z$) to the low temperature Γ_1 ($A_x G_y C_z$) type order of the Fe-sublattice is found at $T_{SR} = 73$ K and does not show any thermal hysteresis. Below $T_{N2} = 4$ K the Dy-sublattice orders in an incommensurate magnetic structure with $k = [0, 0, 0.028]$ while the Fe-sublattice keeps its commensurate Γ_1 type order. DyFeO₃ is the first orthoferrite $R\text{FeO}_3$ to possess an incommensurate magnetic order of the rare earth sublattice under zero field conditions; an important piece of information neglected in the recent discussion of its multiferroic properties.

Keywords: orthoferrites, DyFeO₃, incommensurate magnetic structure, spin reorientation, neutron diffraction

(Some figures may appear in colour only in the online journal)

1. Introduction

The existence of two magnetically ordering sublattices formed by a rare earth (*R*) and by iron and the presence of spin reorientation transitions at strongly varying temperatures put orthoferrites of type $R\text{FeO}_3$ in the focus of research since long times. In fact, the first ever-published paper in *Phys. Rev. Lett.* [1] reported on magnetization results on $R\text{FeO}_3$ compounds and stated already at that point that only in DyFeO₃ the spontaneous magnetization disappears below a certain temperature. Numerous following studies revealed that below T_{N1} ($T_{N1} \sim 600$ – 750 K) and above the spin reorientation transition (T_{SR}) the iron sublattice of all $R\text{FeO}_3$ compounds adopts the so-called Γ_4 ($G_x A_y F_z$) magnetic order [2, 3] with the magnetic

propagation vector $k = 0$. Here we follow the well-known Bertaut notation [4] and use the non-standard $Pbmm$ setting for the description of the magnetic and crystallographic symmetry of these perovskites. The difference between DyFeO₃ and the other $R\text{FeO}_3$ compounds is explained by the fact that while the latter adopt the Γ_2 ($F_x C_y G_z$) type magnetic order below T_{SR} , DyFeO₃ sees a transition to Γ_1 ($A_x G_y C_z$) which no longer possesses a ferromagnetic component. Only very recently, CeFeO₃ was shown to represent a second example of a $\Gamma_4 \rightarrow \Gamma_1$ type transition at T_{SR} in orthoferrites [5]. The presence of a thermal hysteresis at T_{SR} confirmed the first order character of the transition in CeFeO₃, which was in accordance with Yamaguchi's theoretical considerations [3] on spin reorientations in $R\text{Fe}(\text{Cr})\text{O}_3$ compounds. On the other hand, it is interesting to note in this context that macroscopic data [6–8] did not find any hysteresis at T_{SR} for DyFeO₃. The strong influence of the transition metal on the type of spin reorientation

* Author to whom any correspondence should be addressed.

can be seen e.g. on the example of $\text{NdFe}_{0.9}\text{Mn}_{0.1}\text{O}_3$ [9] where a 10% replacement of Fe by Mn changes the $\Gamma_4 \rightarrow \Gamma_2$ found in pure NdFeO_3 to a spin reorientation $\Gamma_4 \rightarrow \Gamma_1$.

The magnetic order of the rare earth sublattice only appears at temperatures T_{N2} much lower than T_{SR} [2] showing that the spin reorientation is not simply related to the onset of the rare earth moment. As the single ion anisotropy of the half-filled shell of the Fe^{3+} ion is small, the magnetic interactions with the rare earth can, however, influence the spin direction even when being still very small [10]. Sivardiére *et al* [11–13] were the first to try to explain the existence of the spin reorientation transitions present only in $R\text{FeO}_3$ compounds hosting magnetic rare earths but absent for non-magnetic $R = \text{Lu}, \text{Eu}, \text{La}, \text{Y}$ and as well absent for the isotropic $R = \text{Gd}$ with $L = 0$. Their work was followed by the very detailed analysis of all the possible magnetic interactions between the iron and the rare earth sublattices by Yamaguchi [3] and the work of Bazaliy *and co-workers* [14, 15]. The possibility to recover the Γ_4 groundstate in DyFeO_3 applying an external magnetic field even below T_{SR} has been first shown by Belov *et al* [16] and further discussed by Eremenko *et al* [17] and later again by Tokunaga *et al* [18]. While the value of T_{SR} has been given as lying between 30 K and 52 K [1, 8, 18–20] from magnetization, spin Hall magnetoresistance and neutron diffraction studies using single crystals, Rajeswaran *et al* [21] found the onset of T_{SR} at 80 K from Mössbauer and magnetization studies on a powder.

Lately, these orthoferrites have regained strong interest due to the discovery of multiferroic properties, as found e.g. in CeFeO_3 [22], SmFeO_3 [23], DyFeO_3 [7, 8, 18, 21, 24, 25] and GdFeO_3 [26] and due to the discovery of ultrafast laser induced spin switching phenomena in e.g. TmFeO_3 [27, 28] DyFeO_3 [29] and ErFeO_3 [30].

In this context, the recent literature on DyFeO_3 [7, 8, 18, 20, 21, 24, 25] assumed without exception that the Dy-sublattice orders as in DyAlO_3 [31] and DyCoO_3 [32] in a commensurate G_xA_y configuration corresponding to Γ_5 for the rare earth $4c$ site. Zhao *et al* [7] postulated an unknown magnetic structure of the Fe-sublattice below T_{N2} to explain a step like increase of the polarization $P(H)$ and irreversible effects in magnetization, polarization and specific heat when cooled in zero magnetic and electric field but did not question the commensurate G_xA_y type order of the Dy-sublattice. Tokunaga *et al* [18] assume the $k = 0$ type magnetic structure of the rare earth sublattice when discussing the strong linear magnetoelectric responses found in DyFeO_3 below T_{N2} . Latest neutron data on a DyFeO_3 single crystal by Wang *et al* [8] were as well interpreted using this model and interpreted the hysteretic effects seen in [7] as linked to a long range to short range order transition of the Dy-sublattice under magnetic field. However, the first neutron study on DyFeO_3 done by Mareschal and Sivardiére in 1969 [12] had clearly indicated that at temperatures below the supposed ordering of the Dy-sublattice an incommensurate magnetic modulation appears. Due to insufficient resolution they were, however, not able to determine the wavevector of the modulation or the spin direction of the

Dy-moment. Apart from this early study and the recent study by Wang *et al* [8] there are no other neutron diffraction data available on DyFeO_3 .

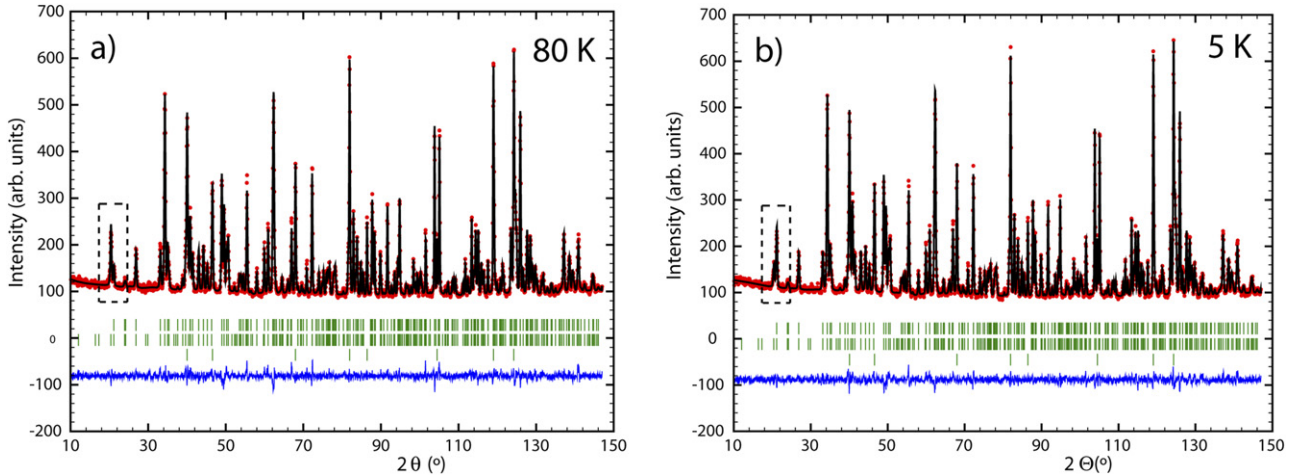
In order to complete the determination of the magnetic order adopted by the Dy-sublattice below T_{N2} and in order to verify whether the Fe-sublattice orders differently below T_{N2} as proposed by Zhao *et al* [7] we decided to perform a detailed temperature dependent neutron diffraction study on a powdered sample of DyFeO_3 .

2. Experimental details

Two ingots of DyFeO_3 were prepared by a vertical floating zone (FZ) method in an optical mirror furnace. The starting materials consisted of high-purity oxides of Dy_2O_3 (purity 99.9%, producer: Chempur), and Fe_2O_3 (purity 99%, producer: Sigma Aldrich). The starting materials were mixed in a stoichiometric ratio, isostatically cold-pressed into rods, and subsequently sintered at 1100 °C for 10 h in air. The FZ ingot growth was performed using a four-mirror optical furnace equipped with 1 kW halogen lamps, a pulling speed of 5 mm h⁻¹, a counter-rotation of both seed and feed rods 30 rpm and a flowing (2 l min⁻¹) air atmosphere. The samples were checked by room temperature x-ray powder diffraction experiment performed on Philips X'Pert Pro MPD diffractometer and were found to be single-phase. The ingots were powdered by ball milling and the finely powdered sample of DyFeO_3 was mixed in a mass ratio of 1:1 with Al powder and filled in a double wall container to reduce the strong absorption of some of the Dy-isotopes. The high intensity powder diffractometer D20 at the Institut Laue Langevin (ILL), Grenoble, France, was used in two different configurations: data were first taken with the germanium monochromator and a take-off angle of 90° with $\lambda = 1.54$ Å at definite temperatures of 1.5 K, 5 K, 10 K, 25 K, 50 K, 80 K and 300 K measuring every pattern for 1 h. This configuration produces data having relatively high resolution while still profiting from a comparatively high intensity neutron beam [33]. Using the same configuration thermal scans were performed on heating and cooling over the spin reorientation transition temperature. Changing the temperature at a speed of 0.01°/26 s, patterns of 10 min were recorded corresponding to a temperature resolution of 0.23 K between adjacent data points. High intensity data were taken using the graphite monochromator at the 42° take-off angle and $\lambda = 2.41$ Å at $T = 1.6$ K and 5 K for 30 min. The temperature evolution over the magnetic transition at T_{N2} was studied using a thermal ramp between 1.7 K and 5 K taking data with a temperature resolution of $\Delta T \sim 0.3$ K between adjacent data points of 10 min. High resolution neutron diffraction data were recorded on the powder diffractometer D2B (as well ILL) at 5 K, 50 K, 80 K, 150 K, 220 K and 300 K using a wavelength of $\lambda = 1.594$ Å. Data were refined using the Rietveld method and the program FullProf [34]. Magnetic symmetry analysis was done with the help of the program BASIREPS [35, 36].

Table 1. Structural details and magnetic moment values of DyFeO₃ as determined from the refinement of high resolution neutron powder diffraction data. Space group *Pbnm* with Dy on Wyckoff site 4c (*x*, *y*, 1/4), Fe on 4b (0, 1/2, 0), O(1) on 4c and O(2) on 8d (*x*, *y*, *z*).

	300 K	220 K	150 K	80 K	50 K	5 K
<i>a</i> (Å)	5.304 82(7)	5.299 42(6)	5.297 62(6)	5.297 17(6)	5.296 97(6)	5.2969(6)
<i>b</i> (Å)	5.597 84(7)	5.593 04(6)	5.591 23(6)	5.590 26(5)	5.590 17(5)	5.5902(5)
<i>c</i> (Å)	7.622 99(8)	7.613 79(8)	7.608 95(8)	7.605 95(8)	7.605 38(8)	7.6051(8)
Dy; <i>x</i>	0.9827(3)	0.9827(2)	0.9819(2)	0.9815(2)	0.9814(2)	0.9818(2)
<i>y</i>	0.0663(2)	0.0669(2)	0.0676(2)	0.0679(2)	0.0675(2)	0.0677(2)
O(1); <i>x</i>	0.1075(7)	0.1072(6)	0.1071(6)	0.1068(6)	0.1072(6)	0.1079(6)
<i>y</i>	0.4606(7)	0.4593(6)	0.4607(6)	0.4592(6)	0.4599(6)	0.4579(6)
O(2); <i>x</i>	0.6944(5)	0.6921(4)	0.6927(4)	0.6924(4)	0.6921(4)	0.6926(4)
<i>y</i>	0.3036(5)	0.3048(4)	0.3029(4)	0.3037(4)	0.3059(4)	0.3040(4)
<i>z</i>	0.0573(3)	0.0564(3)	0.0545(3)	0.0548(3)	0.0567(3)	0.0554(3)
Fe–O(1) (Å)	2.001(1)	1.999(1)	1.997(1)	1.997(1)	1.997(1)	1.999(1)
Fe–O(2) (Å)	2.007(3)	2.010(2)	2.009(2)	2.008(2)	2.006(1)	2.007(1)
	2.035(3)	2.031(2)	2.020(2)	2.024(2)	2.036(1)	2.026(1)
Fe–O(1)–Fe	144.4°(1)	144.4°(1)	144.5°(1)	144.4°(1)	144.4(1)	144.0(1)
Fe–O(2)–Fe	145.1°(1)	144.9°(1)	145.8°(1)	145.5°(1)	144.6(1)	145.3(1)
μ_{Fe} (μ_{B})	3.6(1)	3.9(1)	3.9(1)	4.0(1)	4.0(1)	4.0(1)
R_{B}	4.4	4.5	4.6	4.9	4.2	4.4
R_{Mag}	4.9	5.0	6.6	3.7	4.3	3.8

**Figure 1.** Observed (dots, red), calculated (line, black) and difference patterns of high resolution data of DyFeO₃ from D2B with $\lambda = 1.594$ Å at (a) 80 K and (b) 5 K. The tick marks indicate the calculated position of the nuclear (upper row) and magnetic (middle row) Bragg peaks of DyFeO₃ and of the nuclear Bragg peaks of Al (lower row). The dashed rectangles at low 2Θ values enclose the region where the strongest changes in the magnetic peak intensities exist between the two temperatures.

3. Results and discussion

The refinement of the high resolution D2B data confirms that the structure of the sample has the expected symmetry *Pbnm*. Lattice constants and the most important structural details are listed in table 1 for the six temperatures measured. As the magnetic transition temperature for the ordering of the Fe-sublattice is at about $T_{\text{N1}} \sim 650$ K [19] all data contain already a magnetic contribution. The diffraction lines of the Al powder were treated as a second phase in the refinement. A refinement of the oxygen stoichiometry results in a slight overstoichiometry ($\sim 3(1)\%$), which might indicate some cation vacancies. Due to the contribution of magnetic scattering intensity to the nuclear peaks, the refinement of the exact stoichiometry is, however, not very sensitive to the data and in the following we assumed a stoichiometric sample.

As will be shown later, the spin reorientation transition in this sample can be situated at about $T_{\text{SR}} = 73$ K. Figure 1(a) shows therefore exemplarily refined data measured above T_{SR} at 80 K while figure 1(b) shows refined data taken below T_{SR} at 5 K. In this temperature region only the Fe-sublattice is magnetically ordered and adopts as expected the Γ_4 ($G_x A_y F_z$, magnetic space group $Pb'n'm$, 62.448) magnetic order above T_{SR} and the Γ_1 ($A_x G_y C_z$, magnetic space group *Pbnm*, 62.441) type magnetic order below T_{SR} . Only the *G*-type coupling is of measurable size as the ferromagnetic component of Γ_4 , which can be linked to the Dzyaloshinsky–Moriya interaction, is of the order of $F_z \sim 0.1 \mu_{\text{B}}$ [19]. The *A*-type coupling has only been determined by single crystal neutron diffraction in YbFeO₃ and YFeO₃ [37] and was shown to be of even smaller size. The values of the refined magnetic moment on the Fe-site listed in table 1 therefore correspond to a G_x coupling for $T = 300$ K,

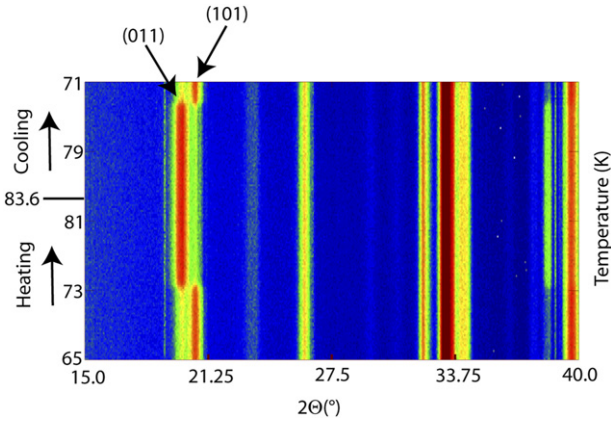


Figure 2. Thermal evolution of the low angle neutron diffraction pattern shown as a contour plot. The changing intensities of the magnetic (011) and (101) reflections indicate the temperature of the spin reorientation on heating and on cooling.

220 K, 150 K and 80 K and to the G_y coupling for $T = 50$ K and 5 K. The results of the refinements show that there are no clear structural changes detectable as the system undergoes the spin reorientation. A slight decrease of the Fe–O(2)–Fe angle when going from 80 K to 50 K is lifted at 5 K and is interpreted as non-real. The values of the Fe–O–Fe angles which determine the size of the super exchange interactions and thereby the onset of the magnetic order of the Fe-sublattice are with about 144° – 145° of the expected order (143°) [38].

The changes of the magnetic order at T_{SR} lead to a change of the intensities of the (101)/(011) reflections at $2\Theta \sim 20^\circ$ (figure 1). This is more clearly visible in the thermal scan (figure 2) measured on D20 using the high resolution 90° take-off angle, $\lambda = 1.54$ Å, configuration. Coming from below T_{SR} at $T = 65$ K the temperature was slowly increased up to 83.6 K where a temperature decrease down again to 71 K was initiated. The spin reorientation transition is clearly visible as a strong change of peak intensities at e.g. around 20° and 38.5° .

Figure 3 displays the averaged position of the (011)/(101) pair of reflections. As the magnetic order of the Fe-sublattice changes from Γ_4 ($G_x A_y F_z$) to Γ_1 ($A_x G_y C_z$) on cooling across the T_{SR} , magnetic scattering intensity is shifted from the (011) reflection (at $2\Theta = 19.7^\circ$) to the (101) reflection (at $2\Theta = 20.4^\circ$) because the G_x type coupling creates a strong magnetic contribution to the (011) reflection while the G_y type coupling leads primarily to magnetic intensity on the (101) reflection. The midpoint of the spin reorientation transition can be determined to $T_{SR} \sim 73.2$ K while the width of the transition is limited to about $\Delta T = 2.5$ K. Comparing the curves determined from the heating and the cooling cycles it can be seen that there is no indication for any thermal hysteresis linked to this spin reorientation.

Yamaguchi [3] discussed theoretically the abrupt Γ_4 to Γ_1 transition and its first order nature in DyFeO_3 . The absence of any thermal hysteresis found here is in accordance with the lack of any anomaly in the specific heat data [6] and the absence of any magneto-structural changes at T_{SR} as inferred from the high resolution diffraction data. This has to be compared to the situation in CeFeO_3 [5] where the similar spin

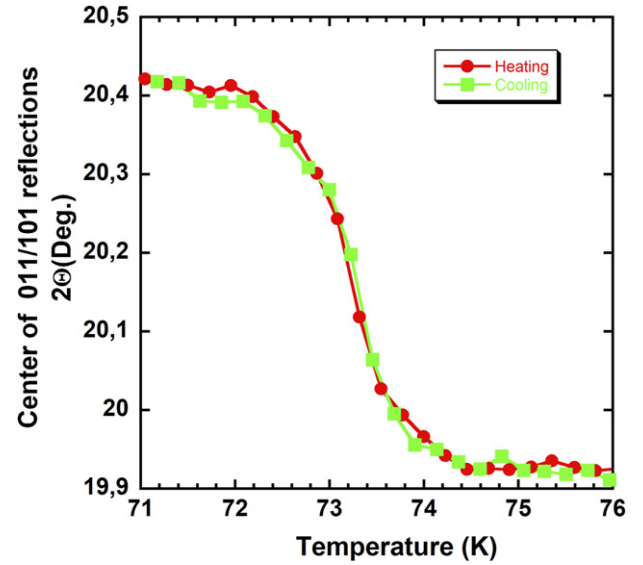


Figure 3. Average position of the pair of magnetic (011)/(101) Bragg peaks which reflects the spin reorientation transition from Γ_4 above T_{SR} to Γ_1 below T_{SR} . Heating and cooling cycles superpose perfectly indicating the absence of a thermal hysteresis of the supposed first order transition. The temperature resolution between adjacent data points is $\Delta T = 0.23$ K.

reorientation $\Gamma_4 \rightarrow \Gamma_1$ is accompanied by a clear thermal hysteresis of about 2.5 K confirming directly the first order nature of the transition. It should, however, be mentioned that even in CeFeO_3 the anomaly found in the specific heat data [39] at the spin reorientation transition ($T_{SR} \sim 230$ K) is only very small and does not allow to specify the first or second order nature of the transition.

No significant changes take place on cooling DyFeO_3 down to 5 K. Below at about 4 K clear changes appear in the neutron diffraction patterns. These changes can be linked to the onset of magnetic order of the Dy-sublattice at T_{N2} previously reported to be in the range 3.7–4.2 K [6–8, 19, 24, 25]. Figure 4 displays the patterns recorded in the high intensity configuration on D20 using $\lambda = 2.41$ Å at 5 K and at the base temperature of 1.6 K. A series of new magnetic peaks appears while those belonging to the magnetic structure adopted by the Fe-sublattice below T_{SR} do not change their intensity. The data resemble those presented in the first low temperature powder neutron study on DyFeO_3 [11] that had not been analysed quantitatively. Using the program K-search which is part of the FullProf suite of programs [34] the new magnetic peaks can be indexed with the magnetic propagation vector $k = [0, 0, l]$ with $l \sim 0.028$. A small peak next to the $(001)^{+k}$ reflection is indexed as the third harmonics $(001)^{+3k}$.

Magnetic symmetry analysis [35, 36] was used to determine the allowed irreducible representations (IRs) and their basis vectors (BVs) for $k = [0, 0, l]$ for the Wyckoff site 4c of Dy (table 2). There are four allowed IRs having each three BVs. This is different to the commensurate case with $k = 0$ where the R-site has eight allowed IRs with each IR having only one or two BVs (see e.g. table 1 of [5]). The coupling of the real part of the IRs between the four R-sites within the unit cell can be described with reference to the notation of Bertaut [4] as

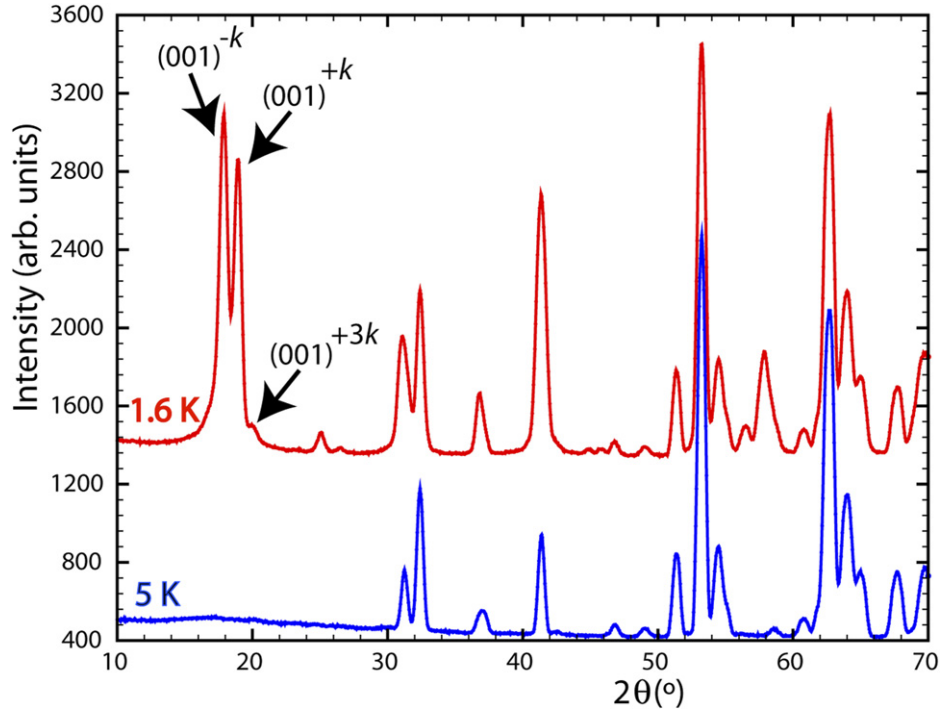


Figure 4. Low angle part of the neutron diffraction patterns of DyFeO₃ at 1.6 K and 5 K. The first magnetic peak at low angles is split into (001)^{+k} and (001)^{-k} with $k = (0, 0, 0.028)$.

Table 2. BVs of the allowed IRs for $k = [0, 0, l]$ for the Wyckoff position 4c of spacegroup *Pbnm*. BASR corresponds to the real part of the BVs while BASI corresponds to the imaginary component. IR2 is highlighted as it represents the IR used for the refinement of the Dy-sublattice order. The IRs are noted as well using the Miller and Love notation^a.

		IR1 (Γ_1), $m\Delta_1$			IR2 (Γ_2), $m\Delta_2$			IR3 (Γ_3), $m\Delta_4$			IR4 (Γ_4), $m\Delta_3$		
		BV1	BV2	BV3	BV1	BV2	BV3	BV1	BV2	BV3	BV1	BV2	BV3
x, y, z	BASR	100	010	001	100	010	001	100	010	001	100	010	001
	BASI	000	000	000	000	000	000	000	000	000	000	000	000
$-x, -y, z+1/2$	BASR	$-a00$	$0-a0$	$00a$	$-a00$	$0-a0$	$00a$	$a00$	$0a0$	$00-a$	$a00$	$0a0$	$00-a$
	BASI	$b00$	$0b0$	$00-b$	$b00$	$0b0$	$00-b$	$-b00$	$0-b0$	$00b$	$-b00$	$0-b0$	$00b$
$-x+1/2, y+1/2, z$	BASR	100	$0-10$	$00-1$	-100	010	001	100	$0-10$	$00-1$	-100	010	001
	BASI	000	000	000	000	000	000	000	000	000	000	000	000
$x+1/2, -y+1/2, z+1/2$	BASR	$-a00$	$0a0$	$00-a$	$a00$	$0-a0$	$00a$	$a00$	$0-a0$	$00a$	$-a00$	$0a0$	$00-a$
	BASI	$b00$	$0-b0$	$00b$	$-b00$	$0b0$	$00-b$	$-b00$	$0b0$	$00-b$	$b00$	$0-b0$	$00b$
Coupling (Bertaut)	BASR	A_x	G_y	C_z	G_x	A_y	F_z	F_x	C_y	G_z	C_x	F_y	A_z

^a $a = \cos(\pi l)$, $b = i \sin(\pi l)$.

$\Gamma_1 \hat{=} A_x G_y C_z$, $\Gamma_2 \hat{=} G_x A_y F_z$, $\Gamma_3 \hat{=} F_x C_y G_z$ and $\Gamma_4 \hat{=} C_x F_y A_z$ (last row of table 2).

Any refinement of the low temperature data has to include four different phases: the nuclear phase of DyFeO₃, the magnetic phase describing the commensurate magnetic order of the Fe-sublattice, the magnetic phase describing the incommensurate magnetic order of the Dy-sublattice and the nuclear phase of the Al-powder. Testing the different IRs against the data taken at 1.6 K it becomes clear that only Γ_2 (BASR: $G_x A_y F_z$) is able to refine the strong new magnetic peaks. The incommensurate magnetic propagation vector refines to $k = [0, 0, 0.0280(1)]$ and the magnetic coupling components of the

Dy-sublattice are $BV1 = 5.0(1) \mu_B$ and $BV2 = 9.1(1) \mu_B$. The third BV which is in principle allowed in Γ_2 can be refined to $BV3 = 1.8(3) \mu_B$, its inclusion in the refinement of the incommensurate phase of Dy leads, however, to a slight increase of the magnetic *R*-factor of this phase. This can be explained by the fact that the small value of l brings the reflections that are most sensitive to the presence of a BV3 component (e.g. $(110)^{\pm k}$) very close to the (110) reflection of the nuclear phase. Furthermore, these $(110)^{\pm k}$ reflections have a much larger contribution coming from the BV1 component resulting in a strong correlation, which questions the reality of the comparatively small BV3 component. We

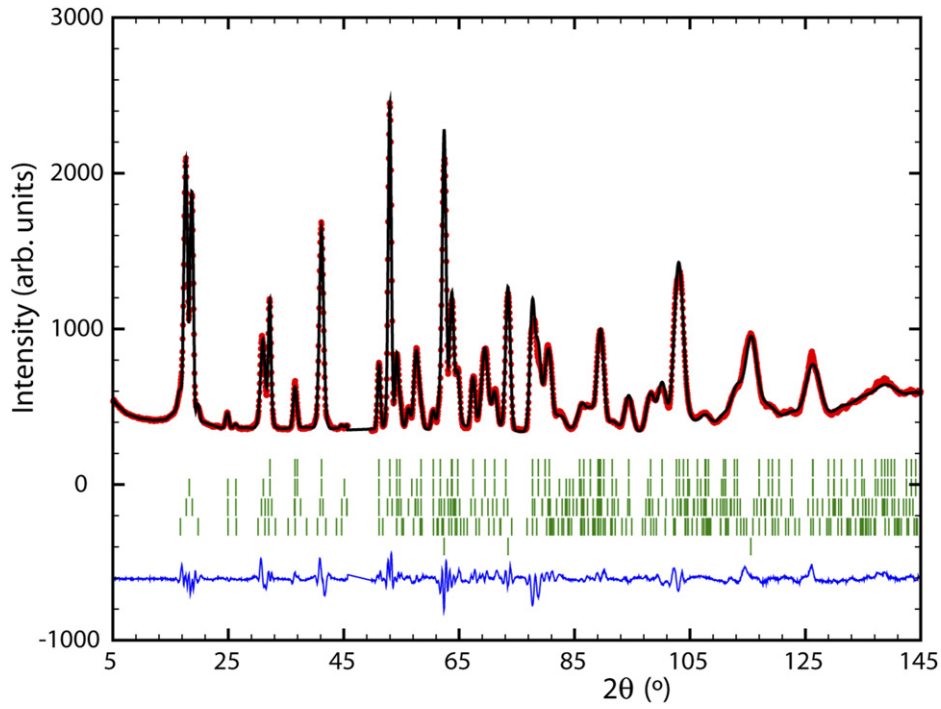


Figure 5. Observed (dots, red), calculated (line, black) and difference patterns of high intensity data of DyFeO₃ from D20 with $\lambda = 2.41$ Å at 1.6 K. The tick marks indicate the calculated position of the nuclear (uppermost row), the commensurate $k = 0$ magnetic (second row) and the incommensurate $k = [0, 0, l]$ (third row) Bragg peaks of DyFeO₃. The fourth row corresponds to the magnetic peaks of the third harmonics of the incommensurate phase while the lowest row corresponds to the nuclear Bragg peaks of Al.

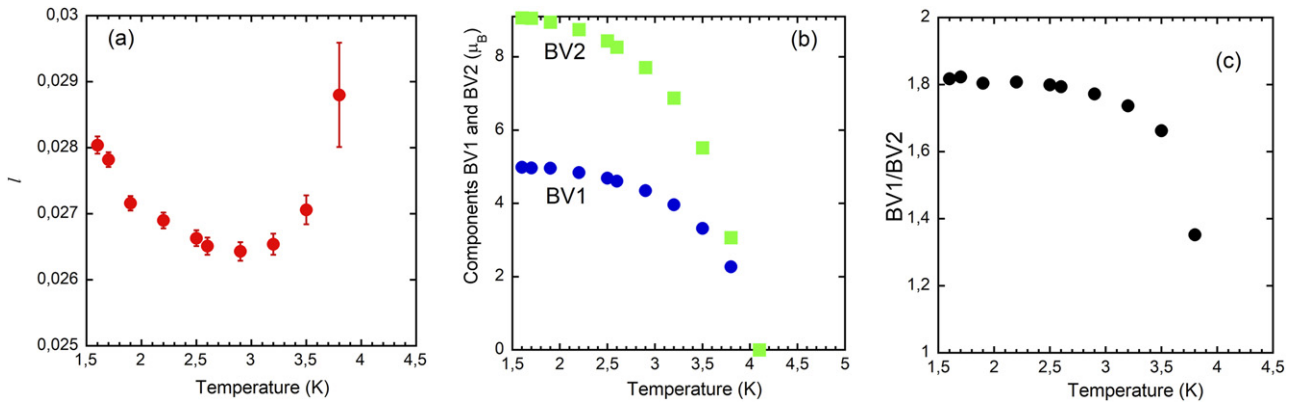


Figure 6. Temperature dependence of (a) the value l of the magnetic propagation vector $k = [0, 0, l]$, (b) the two components of the magnetic order of the Dy-sublattice and (c) the ratio BV1/BV2.

have to recall here the antiferromagnetic nature of the magnetic structure: due to the incommensurate magnetic propagation vector this hypothetical F -coupling (see Γ_2 in table 2, BASR of BV3) would not lead to a detectable macroscopic magnetic moment; in fact a complete reversal of the magnetic moment occurs after a period of $1/0.028 \sim 36$ unit cells. More important than the knowledge about the presence or absence of an F -type coupling is the information that it would be allowed within the same IR. This is different from the magnetic order as supposed in the recent literature [7, 8, 18, 20, 21, 24, 25] for the Dy-sublattice with $k = 0$ and the Γ_5 ($G_x A_y$) model which has no third allowed BV. Figure 5 displays the refinement of the $T = 1.6$ K data ignoring BV3

but including a small contribution from the third harmonics of the $k = [0, 0, l]$ phase (see figure 4 for the $(001)^{+3k}$ reflection).

The magnetic order of the Fe-sublattice does not change below T_{N2} . It keeps the $k_{Fe} = 0$, Γ_1 ($A_x G_y C_z$) type order with $G_y = 3.9(1) \mu_B$ and $A_x = C_z = 0$. Attempts to attribute an incommensurate component to the Fe-sublattice magnetic order failed as much as those to refine an additional $k = 0$ component. This contradicts the idea of having a different magnetic structure of Fe present below T_{N2} that was proposed by Zhao *et al* [7] as possible reason to explain a step like increase of the polarization $P(H)$ after zero field cooling. In this context it is interesting to mention that a change of the magnetic order of the Fe-sublattice below T_{N2} has recently been shown [40] to

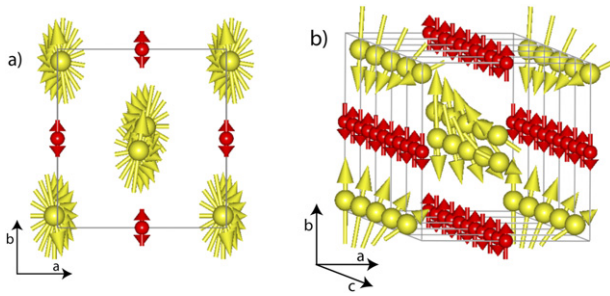


Figure 7. Magnetic structure of DyFeO₃ below T_{N2} : (a) the Dy spins (yellow) form elliptical spirals along the c -axis. (b) Oblique view showing the G_y -type order of the Fe spins (red). The turn angle of the Dy spiral has been upscaled to facilitate the visualization.

actually exist in TbFeO₃, where the Γ_4 order is re-established as the Tb-sublattice changes from the Γ_2 (F_xC_y) to the Γ_8 (A_xG_y) magnetic order below 3 K.

Using single crystal neutron data Wang *et al* [8] have shown that the application of an external magnetic field in c -direction can lead to the re-establishment of the Γ_4 magnetic order for the Fe-sublattice in DyFeO₃ below T_{SR} . T_{SR} itself is progressively reduced with increasing magnetic field strength until it merges with T_{N2} at about $H = 1$ T. At even higher magnetic fields T_{SR} and T_{N2} move to lower temperatures and the magnetic order of the Dy-sublattice becomes of short-range order type. Surprisingly the magnetization, which is induced on the Fe-sublattice by the external field (which is linked to the $\Gamma_4 \hat{=} G_xA_yF_z$ type order), decreases below T_{N2} indicating that the external magnetic field does not have the effect of inducing as well a ferromagnetic component on the Dy-sublattice. The strongly increased magnetic field needed to induce Γ_4 of the Fe-sublattice below T_{N2} indicates instead that the magnetic order of the Dy-sublattice stabilizes the Γ_1 ($A_xG_yC_z$) type order of Fe. This reflects the importance of the magnetic R – M interactions, which are thought to determine as well at zero field the spin reorientation transition from Γ_4 to Γ_1 of the Fe-sublattice. The results of [8] show that magnetic field does not induce a ferromagnetic component on the Dy-sublattice. This could speak against the presence of a significant BV3 component at zero field in the nearly commensurate phase with $k = [0, 0, 0.028]$ discussed above.

Obviously, one has to discuss the fact that Wang *et al* [8] did not find any incommensurability of the Dy-sublattice magnetic order. Two possible origins can be put forward: either this incommensurability does not exist in DyFeO₃ single crystals, or it was overlooked due to insufficient resolution or due to omission of the $(00l)$ reflection family, which is where this incommensurability would most easily be visible. A different behaviour of single crystals and powders became clearly apparent in the different values determined for $T_{SR} \sim 30$ – 50 K for single crystals [1, 8, 18–20] and for powders, $T_{SR} \sim 80$ K [21] and $T_{SR} = 73.2$ K (figure 3). In our powder data the splitting caused by the incommensurability is only clearly visible for the $(001)^{\pm k}$ pair of reflections. Wang *et al* [8] state that due to the presence of two crystalline domains the $(00l)$ reflections measured with zero field were excluded from their refinement. Data taken with magnetic field had been limited

to the $(hk0) \pm 5^\circ$ scattering plane making the detection of any incommensurability along the c -axis impossible. It is highly desirable to repeat a single crystal measurement concentrating on the incommensurability and its possible change as function of magnetic field.

Temperature dependent high intensity data between 1.6 K and 5 K were used to follow the evolution of the incommensurate magnetic propagation vector $k_{Dy} = [0, 0, l]$ and of the magnetic coupling components of the Dy-sublattice. Figure 6(a) shows that the value of l changes slightly having a minimum at about 2.9 K. From figure 6(b) it can be seen that the two components of the Dy magnetic order BV1 and BV2 both disappear at $T_{N2} \sim 4$ K. They have a slightly different temperature dependence as visible in figure 6(c) where the ratio BV1/BV2 shows a nearly constant value up to about 2.6 K before on approaching T_{N2} the BV1 component shows an accelerated decrease. This changing ratio might be the reason for the change of the temperature dependence of k_{Dy} around $T = 2.9$ K (figure 6(a)).

The two BVs of the $k_{Dy} = [0, 0, l]$ Dy magnetic order (table 2) can be combined to describe the magnetic structure either as spin density sinewaves running along the c -direction (magnetic superspace group $Pbnm.1(0,0,g)s00$, 62.1.9.4.m441.1) or as elliptical spirals turning around the c -direction (magnetic superspace group $Pbn2_1.1(0,0,g)s0s$, 33.1.9.2.m144.1). While the first model is centrosymmetric, the second one has lost the centre of inversion. It is not possible to make a difference between both solutions using our powder diffraction data as the magnetic structure factors of the magnetic reflections are practically identical for both models. Sometimes it is nevertheless possible to make a decision between the two solutions by looking at the values of the refined magnetic moments. In our case, where the spin density model leads to a maximum amplitude of the magnetic moment of $\mu_{Dy} = 10.4(2) \mu_B$ while the elliptical spiral model results in $\mu_{Dy} = 5.0$ – $9.1 \mu_B$ it is not possible to exclude a model as the expected free ion value of the magnetic moment of Dy³⁺ amounts to $\mu_{Dy^{3+}} = 10 \mu_B$ and is therefore compatible with both solutions. A parallel or antiparallel alignment of magnetic moments as present in a spin density wave is favoured by isotropic magnetic interactions. Yamaguchi [3] identified the antisymmetric (Dzyaloshinsky–Moriya) and the anisotropic-symmetric magnetic exchange interactions between the rare earth R^{3+} and the Fe³⁺ as driving mechanism for the spin reorientation in orthoferrites. As the R –Fe interactions are generally thought to be stronger than the isotropic magnetic interactions R – R the elliptical spiral model (figure 7) seems more likely but only a neutron diffraction study on a single crystal using full polarization analysis will be able to decide between the two models.

The presence of an incommensurate modulation of the magnetic order on the rare earth sublattice found for DyFeO₃ represents an exception in the class of orthoferrites. This new result should be taken into consideration when discussing the multiferroic effects present below T_{N2} [24–26]. For a single crystal of TbFeO₃ Artyukhin *et al* [40] have shown that magnetic fields along the c -direction induce for $H = 2$ T an incommensurate modulation of the Tb-order within a small temperature

range. This modulation appears below 4 K, runs along the b -unit cell direction with a periodicity of about 340 Å and turns rapidly commensurate at $T \sim 2.75$ K. The authors of [40] explain its existence by interacting periodic domain walls and point to the possible relevance for the interpretation of the spontaneous electric polarization with applied field.

4. Conclusions

Using high intensity and high resolution powder neutron diffraction the magnetic structures of DyFeO₃ have been determined as a function of temperature. The high temperature commensurate ($k_{\text{Fe}} = 0$) magnetic order of the Fe-sublattice undergoes a spin reorientation at $T_{\text{SR}} = 73.2$ K from the Γ_4 ($G_x A_y F_z$) type order to the Γ_1 ($A_x G_y C_z$) type. Along with CeFeO₃ [5], DyFeO₃ is only the second RFeO₃ compound that sees the Γ_1 coupling of Fe below T_{SR} . The value of T_{SR} determined from this powder sample is significantly higher than values determined from single crystal studies ($T_{\text{SR}} \sim 30$ –50 K). Even with a temperature resolution of $\Delta T = 0.3$ K no hysteresis is found although the transition is thought to be of first order. Below $T_{\text{N}2} = 4$ K the magnetic order of the Fe-sublattice does—contrary to a proposition of Zhao *et al* [7]—not change as the Dy-sublattice adopts an incommensurate $k_{\text{Dy}} = [0, 0, l]$ Γ_2 ($G_x A_y F_z$ -type) order. DyFeO₃ is the first example of an RFeO₃ compound possessing an incommensurate order of the rare earth sublattice in zero field conditions. The value of $l \sim 0.028$ changes only very slightly with temperature and leads to a repeat distance of the antiferromagnetic structure of about 36 unit cells along the unit cell c -direction. The incommensurability of the magnetic order of the Dy-sublattice is an important information for the discussion of the multiferroic properties of DyFeO₃ [7, 8, 18, 21, 24, 25] at very low temperatures. Single crystal neutron diffraction data using full polarization analysis will be, however, needed to decide whether the magnetic structure consists of centrosymmetric spin density waves or of elliptical spirals without centre of inversion.

Acknowledgments

ILL is acknowledged for beam time allocation under the experiment code 5-31-2822, doi: <https://doi.org/10.5291/ILL-DATA.5-31-2822>. This work was supported by projects VEGA 2/0011/22. We would like to thank J Rodriguez-Carvajal for his precious help determining the magnetic super-space groups.

Data availability statement

The data generated and/or analysed during the current study are not publicly available for legal/ethical reasons but are available from the corresponding author on reasonable request.

ORCID iDs

Clemens Ritter  <https://orcid.org/0000-0003-3674-3378>
 Joaquim Agostinho Moreira  <https://orcid.org/0000-0003-4659-7503>
 Matus Mihalik  <https://orcid.org/0000-0002-5316-0089>
 Marian Mihalik  <https://orcid.org/0000-0002-5442-9414>
 Stanislav Savvin  <https://orcid.org/0000-0002-2541-909X>

References

- [1] Borzorth R M, Kramer V and Remeika J P 1958 *Phys. Rev. Lett.* **1** 3
- [2] White R L 1969 *J. Appl. Phys.* **40** 1061
- [3] Yamaguchi T 1974 *J. Phys. Chem. Solids* **35** 479
- [4] Bertaut E F 1963 *Magnetism* vol 3 ed G T Rado and H Suhl (New York: Academic) p 149
- [5] Ritter C, Ceretti M and Paulus W 2021 *J. Phys.: Condens. Matter* **33** 215802
- [6] Berton A and Sharon B 1968 *J. Appl. Phys.* **39** 1367
- [7] Zhao Z Y, Zhao X, Zhou H D, Zhang F B, Li Q J, Fan C, Sun X F and Li X G 2014 *Phys. Rev. B* **89** 224405
- [8] Wang J *et al* 2016 *Phys. Rev. B* **93** R140403
- [9] Mihalik M, Roupová P, Tarasenko R, Rams M, Hoser A and Mihalik M 2020 *J. Magn. Magn. Mater.* **502** 166539
- [10] Staub U *et al* 2017 *Phys. Rev. B* **96** 174408
- [11] Sivardiere J 1969 *Solid State Commun.* **7** 1555
- [12] Mareschal J and Sivardière J 1969 *J. Phys. France* **30** 967
- [13] Pataud P and Sivardière J 1970 *J. Phys. France* **31** 1017
- [14] Bazaliy Y B, Tsymbal L T, Kakazei G N, Kamenev V I and Wigen P E 2005 *Phys. Rev. B* **72** 174403
- [15] Tsymbal L T, Bazaliy Y B, Derkachenko V N, Kamenev V I, Kakazei G N, Palomares F J and Wigen P E 2007 *J. Appl. Phys.* **101** 123919
- [16] Belov K P, Zvezdin A K, Kadomtseva A M and Krynetskiĭ I B 1975 *Sov. Phys. JETP* **40** 980
- [17] Eremenko V V, Gnatchenko S L, Kharchenko N F, Lebedev P P, Piotrowski K, Szymczak H and Szymczak R 1987 *Europhys. Lett.* **4** 1327
- [18] Tokunaga Y, Igushi S, Arima T and Tokura Y 2008 *Phys. Rev. Lett.* **101** 097205
- [19] Gorodetsky G, Sharon B and Shtrikman S 1968 *J. Appl. Phys.* **39** 1371
- [20] Hoozeboom G R, Kuschel T, Bauer G E W, Mostovoy M W, Kimel A V and van Wees B J 2021 *Phys. Rev. B* **103** 134406
- [21] Rajeswaran B, Sanyal D, Chakrabarti M, Sundarayya Y, Sundaresan A and Rao C N R 2013 *Europhys. Lett.* **101** 17001
- [22] Hou L, Shi L, Zhao J, Zhou S, Pan S, Yuan X and Xin Y 2019 *J. Alloys Compd.* **797** 363
- [23] Lee J-H, Jeong Y K, Park J H, Oak M-A, Jang H M, Son J Y and Scott J F 2011 *Phys. Rev. Lett.* **107** 117201
- [24] Nakajima T, Tokunaga Y, Taguchi Y, Tokura Y and Arima T-h 2015 *Phys. Rev. Lett.* **115** 197205
- [25] Stanislavchuk T N *et al* 2016 *Phys. Rev. B* **93** 094403
- [26] Tokunaga Y, Furukawa N, Sakai H, Taguchi Y, Arima T-h and Tokura Y 2009 *Nat. Mater.* **8** 558
- [27] Kimel A V, Kirilyuk A, Tsvetkov A, Pisarev R V and Rasing T 2004 *Nature* **429** 850
- [28] Zhang K *et al* 2016 *Sci. Rep.* **6** 23648
- [29] Kimel A V, Kirilyuk A, Usachev P A, Pisarev R V, Balbashov A M and Rasing T 2005 *Nature* **435** 655
- [30] de Jong J A, Kimel A V, Pisarev R V, Kirilyuk A and Rasing T 2011 *Phys. Rev. B* **84** 104421
- [31] Bidaux R and Mériel P 1968 *J. Phys. France* **29** 220

- [32] van Laar B and Elemans A A 1971 *J. Phys.* **32** 301
- [33] Hansen T C, Henry P F, Fischer H E, Torregrossa J and Convert P 2008 *Meas. Sci. Technol.* **19** 034001
- [34] Rodríguez-Carvajal J 1993 *Physica B* **192** 55
- [35] Rodríguez-Carvajal J BASIREPS: a program for calculating irreducible representations of space groups and basis functions for axial and polar vector properties Part of the FullProf Suite of programs available at <http://ill.eu/sites/fullprog/>
- [36] Ritter C 2011 *Solid State Phenom.* **170** 263
- [37] Plakhty V P, Chernenkov Y P and Bedrizova M N 1983 *Solid State Commun.* **47** 309
- [38] Jain A *et al* 2013 *APL Mater.* **1** 011002
- [39] Yuan S J, Cao Y M, Li L, Qi T F, Cao S X, Zhang J C, DeLong L E and Cao G 2013 *J. Appl. Phys.* **114** 113909
- [40] Artyukhin S *et al* 2012 *Nat. Mater.* **11** 694